



Electrical and thermal properties of $\text{Pr}_{0.6}\text{Sr}_{0.4-x}\text{Ag}_x\text{MnO}_3$ ($x = 0.05$ and 0.1) manganite

R. Thaljaoui^{1,2} and D. Szewczyk^{3,*}

¹Laboratoire de Physique Des Matériaux, Faculté Des Sciences de Sfax, Université de Sfax, B.P. 1171, 3000 Sfax, Tunisia

²SUPRATECS, Department of Electrical Engineering and Computer Science, University of Liège, Liège, Belgium

³Institute for Low Temperature and Structure Research, Polish Academy of Science, Wrocław, Poland

Received: 4 October 2019

Accepted: 17 February 2020

Published online:

27 February 2020

© The Author(s) 2020

ABSTRACT

Monovalent silver-doped $\text{Pr}_{0.6}\text{Sr}_{0.4-x}\text{Ag}_x\text{MnO}_3$ manganite has been chosen for the electrical and thermal transport studies. The electrical measurements confirmed a metal–insulator transition around room temperature. For the analysis of the resistivity data, in the high-temperature paramagnetic region, the adiabatic small polaron hopping model was operative. The magnetoresistance studies, under different external magnetic field, showed that the MR peak is located at the metal–insulator transition and ferromagnetic–paramagnetic transition, which is characteristic for an intrinsic magnetoresistance. The thermal conductivity results exhibit a semicrystalline character with grain boundary scattering as a main mechanism limiting the heat transfer in samples. The electrical contribution to the thermal conductivity is relatively small, around 1%, as in most of the manganites. The transition point around room temperature is also visible. The additionally calculated thermal diffusivity parameter shows values of the order typically found in perovskites.

Introduction

The mixed valence perovskite manganites with general formula $\text{T}_{1-x}\text{R}_x\text{MnO}_3$ (T = rare earth cation, R = alkaline earth cation) have attracted the attention of researchers and emerged as potential candidates for technological application. Reason behind it was mostly their possible use for magnetic read write heads, magnetic refrigeration and application in electronic devices. The interest in those materials was reinforced due to their specific features such as metal–insulator transition, ferromagnetic–paramagnetic phase

transition, colossal magnetoresistance (CMR), charge and orbital ordering and lattice degree of freedom [1–7]. The transport and magnetic properties of these materials originate mainly from double exchange (DE) mechanism with mobile e_g electrons of Mn^{3+} ($t_{2g}^3 e_g^1$) moving to the empty e_g orbital of Mn^{4+} ($t_{2g}^3 e_g^0$) via the oxygen p -orbital. This mechanism enhances the ferromagnetic–metallic state (FMM) [8]. However, the paramagnetic–insulator state (PMI) is explained by the strong electron–phonon interaction which is related to the Jahn–Teller (JT) distortion [9]. Several other

Address correspondence to E-mail: d.szewczyk@intibs.pl

mechanisms were considered for studying the physical properties of manganites as super exchange (SE), phase separation and charge ordered (CO) [10–12]. In order to clarify the physics behind phenomena such as CMR and magnetocaloric effect (MCE), many other factors have been considered. It was reported that physical properties of manganites are very dependent on $\text{Mn}^{3+}/\text{Mn}^{4+}$ ratio, which can be easily changed by simple substitution in the rare earth site or Mn site. Such substitution influences the ferromagnetic–paramagnetic Curie transition temperature (T_C) and metal–insulator transition temperature (T_{MI}) [13]. In fact each substitution of a divalent element with a monovalent one converts a Mn^{3+} with the electronic configuration ($3d^4$, $S = 2$) to a Mn^{4+} with the electronic configuration ($3d^3$, $S = 3/2$). As a result, in the e_g band holes are generated, which allows the charge transfer and induces a ferromagnetic coupling between Mn^{3+} and Mn^{4+} ions.

In one of our previous studies, we reported that the substitution by a monovalent atom in $\text{Pr}_{0.6}\text{Sr}_{0.4-x}\text{A}_x\text{MnO}_3$ system can play an important role in physical properties. Moreover, the substitution in Sr site with monovalent Na, K or Ag ($x = 0.05$ to 0.1) induces a second-order phase transition PM–FM around room temperature [14, 15]. The electrical transport studies for $\text{Pr}_{0.6}\text{Sr}_{0.4-x}\text{A}_x\text{MnO}_3$ ($A = \text{Na}, \text{K}$) compounds confirmed a behavior change from the low-temperature metallic-like ($d\rho/dT > 0$) below T_ρ to the insulator-like ($d\rho/dT < 0$) above T_ρ (where T_ρ is a temperature corresponding to the maximum value of resistivity) [16–18]. Moreover, all studied samples do not show a MR peak in vicinity of their Curie temperature around 300 K, and the metal–insulator transition temperature T_{MI} is observed around 200 K, which is about 100 K below Curie temperature T_C . Interestingly, there are not many reports on doped manganites that exhibit the coincidence of T_C with T_{MI} around room temperature as shown in the case of $\text{Pr}_{0.6}\text{Sr}_{0.4-x}\text{Ag}_x\text{MnO}_3$ ($x = 0.05$ and 0.1). This motivated us to look into electrical and thermal conductivities of monovalent Ag doping in Sr site of $\text{Pr}_{0.6}\text{Sr}_{0.4}\text{MnO}_3$ manganite. It is found that T_{MI} is observed around Curie temperature and slightly increasing with an increasing magnetic field from 0 to 3 T. In order to elucidate the conduction mechanisms, the temperature variation of resistivity was compared with two models above the insulator to metal transition temperature, namely the small polaron hopping (SPH) and Mott's variable range hopping

(VRH), and at low temperature (in the metallic behavior region): electron–electron and electron–magnon scattering processes. Although the electronic transport has been the focus of studies in these systems systematically, the thermal transport has not yet attracted a proper attention. The relatively high electrical resistivity in various types of manganites entails that the dominant mechanism in a ferromagnetic–metallic phase should be the lattice heat conduction. In fact, thermal conductivity κ is a property that reflects scattering of phonons and electrons in a material, which makes it an additional or sometimes also an alternative probe to study the complexity of the CMR phenomena. Survey through the studies on doped manganites shows two types of major behaviors [19, 20]. In the paramagnetic phase, κ is rather of a low value and exhibits an amorphous-like character of the temperature dependence ($d\kappa/dT > 0$). In the ferromagnetic–metallic phase, the observed curves change to the crystalline like ($d\kappa/dT < 0$). The transition between the phases and simultaneously alternation of the thermal transport type results in a minimum at T_C . Usually, as a reason behind this phenomena the distortion of the MnO_6 octahedra is given.

Materials and methods

Polycrystalline $\text{Pr}_{0.6}\text{Sr}_{0.4-x}\text{Ag}_x\text{MnO}_3$ ($x = 0.05$ and 0.1) manganites were prepared by using the conventional solid–state method. The detailed description of samples can be found in Ref. [21]. The electrical resistivity measurements were carried out on PPMS (physical Property Measurement System) from Quantum Design in applied magnetic fields up to 3 T over temperature range 20–340 K using the four probe method. The thermal conductivity measurements were performed on a specially designed heat bath cryostat using the uniaxial steady-state heat flow method in a temperature range 4.2–300 K. The upper limit of measurement was defined by the restrictions of the experimental setup. The precise description of the technique as well as the used cryostat can be found elsewhere [22].

Results and discussion

Electrical resistivity measurements and conduction models

The temperature dependence of electrical resistivity data of $\text{Pr}_{0.6}\text{Sr}_{0.4-x}\text{Ag}_x\text{MnO}_3$ ($x = 0, 0.05$ and 0.1) without and under an applied field up to 3 T is shown in Figs. 1 and 2.

For both investigated samples, resistivity $\rho(T)$ changes from the low-temperature metallic-like behavior ($d\rho/dT > 0$) below T_ρ to the semiconductor-like ($d\rho/dT < 0$) above T_ρ , where temperature T_ρ corresponds to the temperature point, at which resistivity reaches its maximum value. The metal–insulator transition temperature (T_{MI}) is observed around room temperature for both samples. For $\text{Pr}_{0.6}\text{Sr}_{1-x}\text{Ag}_x\text{MnO}_3$ with Ag $x = 0.05$, T_{MI} is just a little lower comparing to the more doped sample. Because of the very subtle change, both in stoichiometry and shift of the T_{MI} , the difference is assigned to the sample morphology. With increasing magnetic field (from 0 to 3 T), metal–insulator transition temperature rises up to about 20 K toward high temperatures. The magnitude of the resistivity is observed to decrease with increase in magnetic field for a whole temperature range. In fact, the presence of an external magnetic field reduces electron scattering at grain boundaries and results in a new orientation of magnetic moments toward the applied field, thereby decreasing the magnetic disorder. As a result, local ordering of the electron spins influences

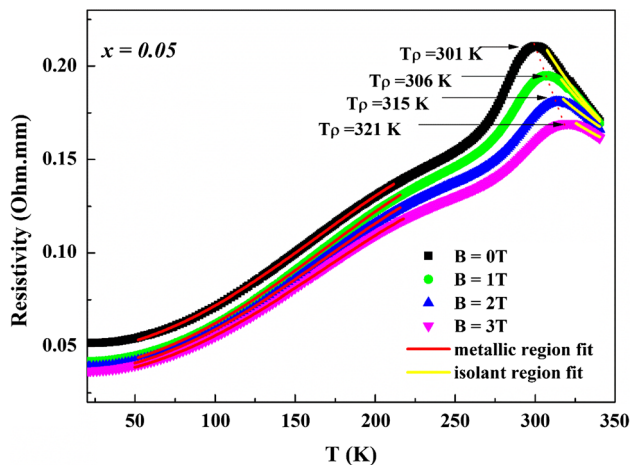


Figure 1 The temperature dependence of resistivity without and under a magnetic field up to 3 T for $\text{Pr}_{0.6}\text{Sr}_{0.35}\text{Ag}_{0.05}\text{MnO}_3$ samples. Inset shows the fitting above and below T_{MI} .

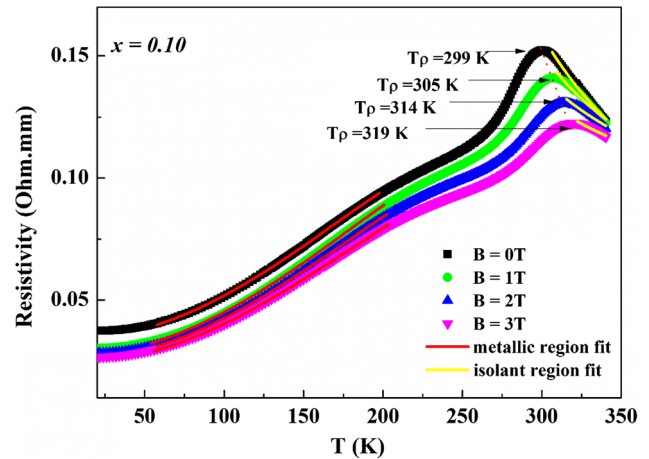


Figure 2 The temperature dependence of resistivity without and under a magnetic field up to 3 T for $\text{Pr}_{0.6}\text{Sr}_{0.3}\text{Ag}_{0.1}\text{MnO}_3$ samples. Inset shows the fitting above and below T_{MI} .

the ferromagnetic metallic state and is followed by the suppressing of the paramagnetic insulating regime leading to the observed increase in T_{MI} . The ferromagnetic alignment, which is due to the double exchange mechanism, causes a decrease in resistivity. In comparison with the previously reported results for monovalent doped $\text{Pr}_{0.6-x}\text{Bi}_x\text{Sr}_{0.4}\text{MnO}_3$ ($x = 0-0.15$) [23], the present one shows a smaller resistivity values under lesser applied magnetic field and a higher metal–insulator transition temperature. It is worth to notice that the resistivity values reported for sample $x = 0.05$ are found to be larger than those reported for $x = 0.1$ sample. Such difference can be explained by grain sizes of particles for each samples. The preliminary studies claimed that the sample with silver amount equal to $x = 0.05$ contains smaller grains (which size varies between 1 and 1.3 μm) compared to those of $x = 0.1$ sample (grain size from 1.3 to 1.8 μm) [24]. The resistivity values were found to be smaller for sample with larger grains. It could be related to the fact that grain boundaries consist more of magnetic disorder and enhance electron scattering. In order to correlate the obtained results with other praseodymium strontium manganites (doped either on the praseodymium or the strontium site), the resistivity values at the metal–insulator transition point at 0 T and 1 T are summarized in Table 1. The included summary manifests also the strong influence of the preparation procedure (sample morphology) and dopants impact on the T_{MI} , changing over 40 K for the pure sample from

Table 1 Comparison of resistivity values at T_{MI} in differently doped PrSrMnO₃

Sample	ρT_{MI} (Ω -mm)		T_{MI} (K)	
	$H = 0$ T	$H = 1$ T	$H = 0$ T	$H = 1$ T
Pr _{0.6} Sr _{0.4} MnO ₃ [16]	0.23	0.21	184	194 K
Pr _{0.6} Sr _{0.35} Ag _{0.05} MnO ₃	0.18	0.17	301	306 K
Pr _{0.6} Sr _{0.3} Ag _{0.1} MnO ₃	0.15	0.14	299	305 K
Pr _{0.6} Sr _{0.35} K _{0.05} MnO ₃ [16]	1.95	1.82	175	194 K
Pr _{0.6} Sr _{0.3} K _{0.1} MnO ₃ [16]	1.65	1.55	170	194 K
Pr _{0.6} Sr _{0.35} Na _{0.05} MnO ₃ [25]	0.83	0.74	165	182 K
Pr _{0.55} Na _{0.05} Sr _{0.4} MnO ₃ [17]	0.38	0.36	104	114 K
Pr _{0.55} K _{0.05} Sr _{0.4} MnO ₃ [18]	0.69	0.67	194	197 K
Pr _{0.45} Bi _{0.15} Sr _{0.4} MnO ₃ [23]	~ 0.44	–	175	–
Pr _{0.6} Sr _{0.4} MnO ₃ [23]	~ 0.19	–	222	–

184 to 222 K [16, 23] and doped ones from 104 [17] to ~ 300 K in our case of silver-doped manganite.

Low-temperature behavior ($T < T_{\rho}$)

At low temperature ($T < T_{\rho}$), in ferromagnetic-metallic phase, the electrical resistivity data have been numerically approximated with a following polynomial equation (an empirical one):

$$\rho = \rho_0 + \rho_2 T^2 + \rho_{4.5} T^{4.5} \quad (1)$$

where ρ_0 is the residual resistivity arising from the temperature-independent processes such as domain wall, grain boundary and vacancies, $\rho_2 T^2$ describes the electron–electron scattering, and $\rho_{4.5} T^{4.5}$ contributes the combination of electron–electron, electron–magnon and electron–phonon scattering process in FM state [26–28]. The obtained values from the best fits of the resistivity data are summarized in Table 2.

We have noticed that with an increasing magnetic field from 0 up to 3 T, the parameters are reducing their values. This could be explained by the overall reduction of the spin fluctuation in the presence of an external magnetic field. Moreover, the obtained values indicate that for each particular temperature in the fitted range the term $\rho_2 T^2$ is larger than the term

$\rho_{4.5} T^{4.5}$ which confirms that in the metallic phase the transport mechanism is governed by the electron–electron scattering.

High-temperature behavior ($T > T_{\rho}$)

Above T_{ρ} , the behavior of electrical resistivity as a function of temperature is explained usually by the adiabatic small polaron (SP) model [28], which is described by the following equation:

$$\rho(T) = BT \exp\left(\frac{E_a}{k_B T}\right) \quad (2)$$

where E_a is the activation energy and B is the residual resistivity coefficient. The E_a values are determined from the best fit of plot $\ln(\rho/T)$ versus $1/T$ (not included in the paper).

The parameters resulting from the best fit, summarized in Table 3, indicate that E_a values are found to be decreasing with increasing magnetic field. This relation could be attributed to a reduction of the charge localization and spin alignment. Following the dopant content, the differences between the activation energies are very subtle, just a bit higher for the $x = 0.1$ sample, probably stemming from the sample microstructure. A similar effect induced by an external magnetic field was previously reported for

Table 2 Approximation parameters of the low temperature resistivity data of Pr_{0.6}Sr_{0.4-x}Ag_xMnO₃ ($x = 0.05$ and 0.1) according to the empirical Eq. (1)

H (T)	ρ_0 (Ω -mm)		ρ_2 (10^{-6} Ω mm/K ²)		$\rho_{4.5}$ (10^{-13} Ω mm/K ^{4.5})	
	$x = 0.05$	$x = 0.1$	$x = 0.05$	$x = 0.1$	$x = 0.05$	$x = 0.1$
0	0.046	0.03356	2.64	1.89	– 9.51	– 6.46
1	0.037	0.026	2.62	1.86	– 8.41	– 5.76
2	0.034	0.025	2.5	1.79	– 8.43	– 5.72
3	0.032	0.023	2.36	1.69	– 8.05	– 5.41

Table 3 Activation energies

E_a deduced from electrical resistivity of $\text{Pr}_{0.6}\text{Sr}_{0.4-x}\text{Ag}_x\text{MnO}_3$ ($x = 0.05$ and 0.1)	H (T)		E_a (meV)	
			$x = 0.05$	$x = 0.1$
	0		58	59
	1		50	55
	2		43	45
	3		39	41

similar manganite systems— $\text{Pr}_{0.55}\text{Na}_{0.05}\text{Sr}_{0.4}\text{MnO}_3$; $\text{Pr}_{0.55}\text{K}_{0.05}\text{Sr}_{0.4}\text{MnO}_3$ [17, 18]. Another example of the suppression of transport energy barriers under the influence of magnetic field has been observed in $\text{Pr}_{0.6}\text{Sr}_{0.4-x}\text{K}_x\text{MnO}_3$ [16].

Magnetoresistance

As noted earlier, the application of external magnetic field suppresses the spin fluctuations and consequently leads to a decrease in the electrical resistivity associated with the magnetic disorder. The influence of a magnetic field is described by the magnetoresistance effect (MR), which can be defined as follows:

$$\text{MR}(T) = \frac{\Delta\rho}{\rho} = \frac{\rho(H) - \rho(0)}{\rho(0)} \quad (3)$$

where $\rho(H)$ and $\rho(0)$ are the resistivities at magnetic field H of 1, 2 and 3 T and at zero field, respectively. The temperature dependence of magnetoresistance (MR) of both samples is shown in Figs. 3 and 4 at different applied magnetic fields.

For both samples, the plots show a peak around room temperature. Their Curie temperatures are

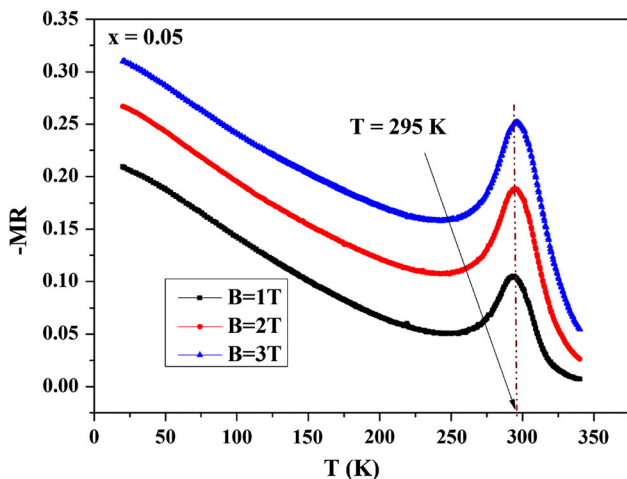


Figure 3 The temperature dependence of magnetoresistance with a magnetic field up to 3 T of $\text{Pr}_{0.6}\text{Sr}_{0.35}\text{Ag}_{0.05}\text{MnO}_3$ sample.

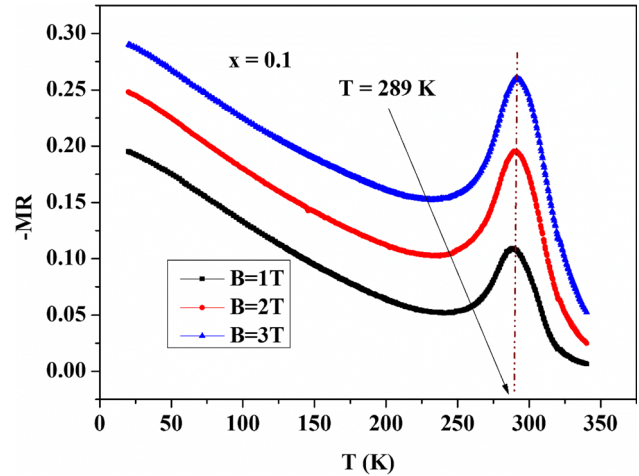


Figure 4 The temperature dependence of magnetoresistance with a magnetic field up to 3 T of $\text{Pr}_{0.6}\text{Sr}_{0.3}\text{Ag}_{0.1}\text{MnO}_3$ sample.

295 K and 289 K for $x = 0.05$ and $x = 0.1$, respectively. The observed decrease in T_c with increase in silver content is derived indirectly from the microstructure of particular samples. For $x = 0.1$, grain boundaries (average sample grain size up to 1.8 μm) generate more magnetic disorder and in that way enhance the electron scattering, which in result influence the FM–PM transition temperature and slightly decrease the T_c when comparing to $x = 0.05$ sample (with av. grain size 1–1.3 μm).

One should also note that the maximum negative MR shows a slight decrease when increasing Ag amount from 0.05 to 0.1. This could be explained by a decrease in the resistivity when increasing Ag content. Whereas with increasing magnetic field from 1 to 3 T, the negative MR values observed around room temperature are found to be from 10 to 26% for both samples. In comparison with previous studies on Na- and K-doped manganites [16, 17] they reach very high values. The former case we reported showed largest MR values around 25 K followed by a gradual decrease with increasing temperature. The characteristic T_{MI} temperature of those compounds was around 200 K, which is about 100 K below the Curie temperature. Venkataiah et al. [26] proposed that the high MR at low temperature can be related to the extrinsic MR effect involving spin-polarized tunneling between grains or spin-dependent scattering of polarized electrons at grain boundaries. Our samples (the silver-doped ones) show a different MR behavior compared to reported previously [16–18], which is determined by the substantially bigger grain

size of the samples (from 1 μm up to 1.8 μm in Ag-doped whereas ~ 50 nm in K-doped and from 400 to 700 nm in Na-doped ones). Many studies have shown that the microstructure modification strongly influences the extrinsic magnetoresistance [29, 30]. The location of the MR peak at metal–insulator temperature transition and ferromagnetic–paramagnetic transition is typical for a different kinds of effect—namely the intrinsic magnetoresistance. The intrinsic MR requires strong magnetic field exceeding 1 T, which in turn suppresses the magnetic disorder and reduces the electron scattering at grain boundaries.

Thermal conductivity

The temperature dependence of thermal conductivity for $\text{Pr}_{0.6}\text{Sr}_{0.4-x}\text{Ag}_x\text{MnO}_3$ ($x = 0.05$ and 0.1) is shown in Fig. 5.

The measured quantities cannot be outright assigned to the amorphous or crystalline type (even though the investigated samples were ceramic pellets). The κ value is monotonically increasing with temperature throughout the investigated temperature range— $d\kappa/dT > 0$, but with different intensity in particular ranges, what would suggest an amorphous type of behavior. However, the magnitude of $\kappa(T)$ lies in the range 0.4–3.4 W/mK, which is a little higher than typical amorphous material [31]. The observed value of thermal conductivity can be attributed to the presence of JT distortions [19, 31]. Below 15 K, the thermal conductivity in both samples is practically equal. For higher temperatures, $\kappa(T)$ of the less doped sample has bigger values. With

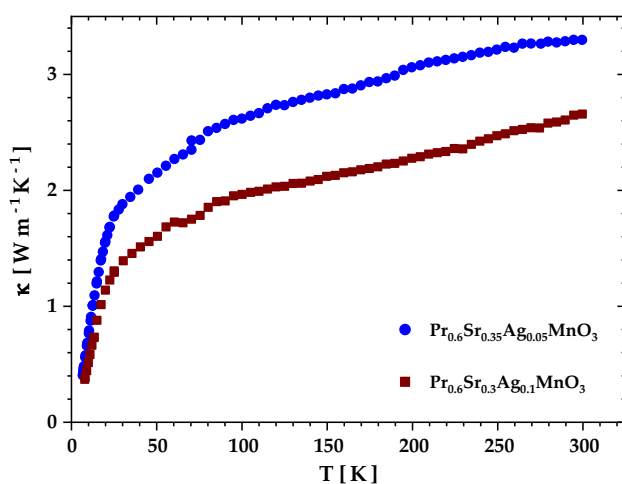


Figure 5 Thermal conductivity of $\text{Pr}_{0.6}\text{Sr}_{0.4-x}\text{Ag}_x\text{MnO}_3$ samples with different silver content as a function of temperature.

increasing silver content, thermal conductivity gets smaller to exceed at room temperature $\kappa_{\text{RT}} = 2.65$ W/mK for $\text{Pr}_{0.6}\text{Sr}_{0.3}\text{Ag}_{0.1}\text{MnO}_3$ and 3.4 W/mK for $\text{Pr}_{0.6}\text{Sr}_{0.35}\text{Ag}_{0.05}\text{MnO}_3$, respectively. The difference in thermal conductivity coefficient is about 30%, which is substantial considering the relatively small difference in the dopant amount. Lowering of the κ value induced by increasing the dopant amount was also observed substituting bismuth in place of praseodymium in $\text{Pr}_{0.6-x}\text{Bi}_x\text{Sr}_{0.4}\text{MnO}_3$ studies [23]. The decrease in magnitude of $\kappa(T)$ is connected to the increased phonon scattering from JT distortion as formation of JT polarons may act as scattering centers. Collating our results with studies of Gamzatov et al. [32] for the pure sample, $\text{Pr}_{0.6}\text{Sr}_{0.4}\text{MnO}_3$ one notes the same type of unusual behavior of the curve $\kappa(T)$ in a wide temperature range. Likewise, the magnitude of the thermal conductivity parameter is kept at the same level (from ~ 1.2 W/mK at 80 K up to ~ 2.6 W/mK just below T_c). Also in the thermal conductivity studies of a different silver-doped lanthanum manganite [33], the same type of $d\kappa/dT > 0$ dependences are demonstrated. As mentioned earlier, given the setup restriction and the fact that T_c of Ag-doped praseodymium strontium manganite is close to room temperature, thermal conductivity beyond T_c in the paramagnetic phase could not be investigated. The only phase for which the measurement was conducted was the ferromagnetic metallic phase.

Because of a high electrical resistivity, one should consider the effect of the electronic contribution to the total thermal conductivity κ_{el} . Under the circumstances of investigating solely the ferromagnetic metallic phase, we can omit the considerations of correctness of the Wiedemann–Franz law (WFL) [34] and assume:

$$\kappa_{\text{el}} = \rho^{-1} L_0 T \quad (4)$$

where $L_0 = 2.45 \cdot 10^{-8}$ W Ω/K^2 (the Lorenz number) and ρ is the resistivity. The results of the calculations from resistivity data are plotted in Fig. 6 (range 20–340 K).

Owing to the extended range (toward high temperatures), one can outright see the minimum connected to the PM–FM transition around room temperature. From exclusively the thermal conductivity results, it was not possible to see the changes in temperature dependence of the κ parameter. The slope of the electrical contribution to the thermal

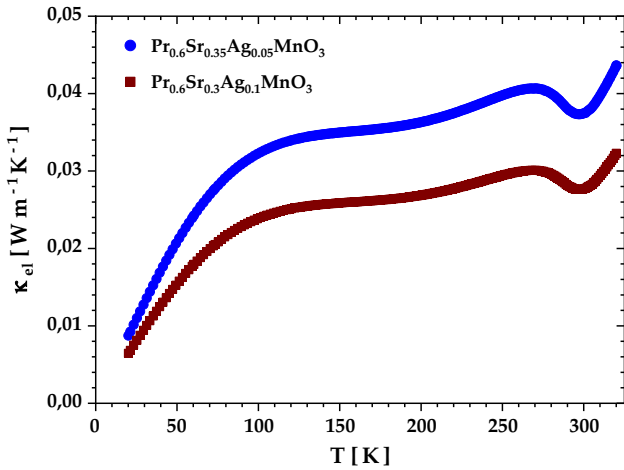


Figure 6 Temperature dependence of electrical contribution to thermal conductivity of $\text{Pr}_{0.6}\text{Sr}_{0.4-x}\text{Ag}_x\text{MnO}_3$ samples with different silver content.

conductivity in the paramagnetic phase is roughly the same for both samples. In the ferromagnetic–metallic phase, the electrical contribution to the total thermal conductivity is kept around 1% at all temperatures. In our particular case, we will skip the considerations of other contributions to the heat conductions like, e.g., from spin waves. The investigated range (not the calculated electronic contribution) ends exactly at the PM–FM transition point, which makes it impossible to proceed with the data analysis in that vicinity.

After subtracting the electronic contribution from the total thermal conductivity, the main heat conducting source remains the lattice conductivity:

$$\kappa_{\text{latt}} = \kappa - \kappa_{\text{el}} \tag{5}$$

In the ferromagnetic region, the lattice thermal conductivity of $\text{Pr}_{0.6}\text{Sr}_{1-x}\text{Ag}_x\text{MnO}_3$ is dominated by phonons, allowing to analyze the low-temperature data on the basis of the relaxation time method [35]. The phonon thermal conductivity is defined as follows:

$$\kappa_{\text{ph}} = \frac{3dnRT^3}{M\theta_D^3} v^2 \int_0^{\theta_D/T} \frac{x^4 e^x}{(e^x - 1)^2} \tau_{\text{ph}} dx, \tag{6}$$

where d —mass density; M —molecular weight; n —number of atoms in the chemical formula of the compound; R —gas constant; θ_D —Debye temperature; $x = \omega_D/T$ —reduced phonon frequency. The phonon relaxation time τ_{ph} is given by:

$$\tau_{\text{ph}}^{-1} = \tau_b^{-1} + KTx + sT^2x^2 + pT^4x^4, \tag{7}$$

where τ_b corresponds to scattering time due to grain boundaries ($\tau_b = l_b/v_{\text{ph}}$, l_b —average crystalline size, v_{ph} —phonon velocity); K is a phonon scattering rate proportional to ω_{ph}^1 , corresponding to scattering by strain fields around dislocation; s —proportional to ω_{ph}^2 —is scattering by sheet like faults; p —proportional to ω_{ph}^4 —is scattering by point defects. As mentioned above, the magnon contribution is neglected, because the phonon–spin scattering has the largest effect near T_c and here the low temperature (away from T_c) is considered. Using the above equation, the fit of the phonon (lattice) thermal conductivity was calculated (for temperatures 20–150 K). The results are shown in Fig. 7. The parameters corresponding to the best fits are summarized in Table 4.

The most striking observation is that independently from the sample type the main mechanism governing and limiting the thermal transport in investigated manganites is the scattering on grain boundaries, which reflect the microstructure of the sample connected to the preparation procedure.

Thermal diffusivity

Thermal diffusivity is a parameter defining the ability of a material to conduct heat. It can be measured directly, e.g., by pyroelectric calorimeter or a laser flash method or can be calculated from the

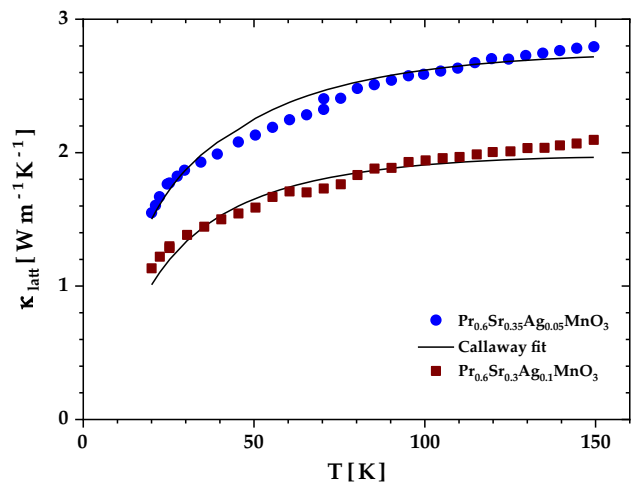


Figure 7 Lattice thermal conductivity of $\text{Pr}_{0.6}\text{Sr}_{0.4-x}\text{Ag}_x\text{MnO}_3$ with different silver content in temperature dependence.

Table 4 Parameters of the Callaway approximation of lattice thermal conductivity of $\text{Pr}_{0.6}\text{Sr}_{0.4-x}\text{Ag}_x\text{MnO}_3$ ($x = 0.05$ and 0.1) samples

Sample	c_s (m/s)	θ_D (K)	$D_{\text{dis}} \cdot 10^7$	$C_{\text{imp}} \cdot 10^3$ (s ³)	$B \cdot 10$ (s/K)	E_U (K)	$A \cdot 10^9$ (s)
$\text{Pr}_{0.6}\text{Sr}_{0.35}\text{Ag}_{0.05}\text{MnO}_3$	5000	598	1.16	4.217	32.48	24.29	2.49
$\text{Pr}_{0.6}\text{Sr}_{0.3}\text{Ag}_{0.1}\text{MnO}_3$	5000	598	1.46	4.160	45.66	33.72	6.54

experimental data of thermal conductivity and heat capacity using the formula below:

$$\alpha(T) = \kappa(T)/\rho\Delta C_p(T), \quad (8)$$

where κ —thermal conductivity coefficient, C_p —heat capacity and $\rho = 6.44 \text{ kg/m}^3$ —density of a material. The estimated values based on heat capacity results from our previous paper [21] are presented in Fig. 8.

The parameter exhibits a monotonic decrease in the value with increasing temperature due to the reduction in phonon mean free path by phonon–phonon scattering. At the lowest temperatures, the diffusivity drops rapidly and stabilizes around 50 K and furthermore continues to decrease smoothly with a very flat slope mirroring, the behavior noted for the undoped sample [32]. One anomaly is observed at high temperatures, which is connected to the paramagnetic–ferromagnetic transition. The temperature dependence of the thermal diffusivity in the vicinity of the PM–FM is shown in Fig. 9.

Changing the scale allowed to visualize the transition. At room temperature, thermal diffusivity is $1.1 \text{ mm}^2/\text{s}$ and $0.91 \text{ mm}^2/\text{s}$ for $\text{Pr}_{0.6}\text{Sr}_{0.4-x}\text{Ag}_x\text{MnO}_3$ $x = 0.05$ and $x = 0.1$, respectively, which lies between the values $\sim 0.8 \text{ mm}^2/\text{s}$ (reported for the undoped sample $\text{Pr}_{0.6}\text{Sr}_{0.4}\text{MnO}_3$ [32]) and $\sim 1.35 \text{ mm}^2/\text{s}$

(reported for PrMnO_3 by Oleaga et al. [36]). The differences in thermal diffusivity might be the result of this property's nature, as it is strongly dependent on the quality of the material (stoichiometrically and crystallographically)—the better the crystal the higher diffusivity value. Considering the observed transition point, it is slightly shifted toward high temperatures when comparing to our previous studies [21] and the diffusivity studies of Gamzatov et al. being just below the room temperature.

Conclusion

The electrical and thermal properties of $\text{Pr}_{0.6}\text{Sr}_{0.4-x}\text{Ag}_x\text{MnO}_3$ ($x = 0.05$ and 0.1) manganite have been reported. The electrical investigations show that both samples exhibit a metal–insulator transition T_{MI} around room temperature. The application of an external magnetic field up to 3 T leads to a new magnetic moment orientation and reduction of spin fluctuation. Addition of a magnetic field increases T_{MI} about 20 K and decreases the resistivity values in the whole temperature range 20–340 K. The resistivity values reported for sample $x = 0.05$ are found to be larger than those reported for $x = 0.1$ sample due

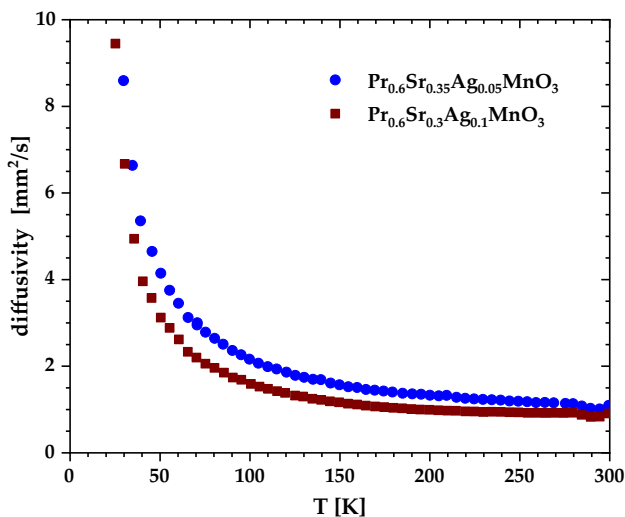


Figure 8 Thermal diffusivity of $\text{Pr}_{0.6}\text{Sr}_{0.4-x}\text{Ag}_x\text{MnO}_3$ with different silver content.

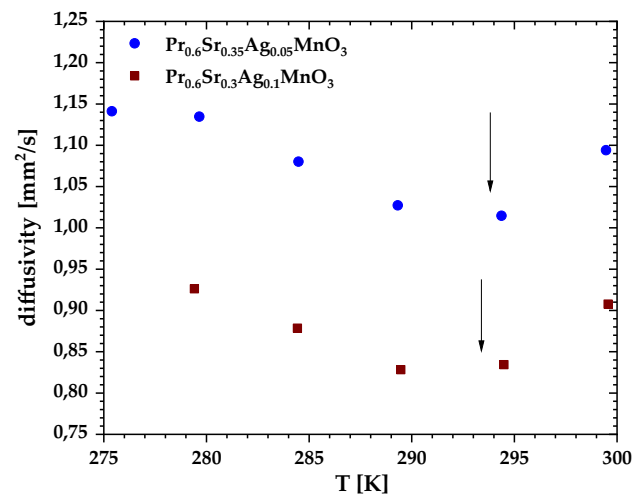


Figure 9 Thermal diffusivity of $\text{Pr}_{0.6}\text{Sr}_{0.4-x}\text{Ag}_x\text{MnO}_3$ in the vicinity of PM–FM transition.

to the grain size of particles. The analysis of resistivity data confirmed that adiabatic small polaron (SP) model is operative above the metal–insulator temperature transition, whereas electron–electron, electron–magnon and electron–phonon scattering processes govern the low-temperature metallic behavior. The temperature dependence of magnetoresistance for both samples shows an intrinsic magnetoresistance behavior with MR peak location at metal–insulator temperature transition and ferromagnetic–paramagnetic which is different to those reported previously [16–18]. The thermal transport studies show semicrystalline properties with values common in perovskite manganites group of materials. From the extracted lattice contribution, the main factor limiting the heat transfer was defined to stem from grain boundaries, supporting the conclusion about strong influence of the sample morphology. The electrical contribution to thermal conductivity exhibits less than 1% of the total thermal conductivity, and the evidence of the PM–FM phase transition is observed around room temperature. The thermal diffusivity parameter decreases with increasing temperature in the whole investigated temperature range (abruptly at low temperatures, above 50 K very smoothly) resembling the values of other perovskite manganites.

Compliance with ethical standards

Conflict of interest The authors declare that they have no conflict of interest.

Open Access This article is licensed under a Creative Commons Attribution 4.0 International License, which permits use, sharing, adaptation, distribution and reproduction in any medium or format, as long as you give appropriate credit to the original author(s) and the source, provide a link to the Creative Commons licence, and indicate if changes were made. The images or other third party material in this article are included in the article's Creative Commons licence, unless indicated otherwise in a credit line to the material. If material is not included in the article's Creative Commons licence and your intended use is not permitted by statutory regulation or exceeds the permitted use, you will need to obtain permission directly from the copyright holder. To view a copy of this licence, visit <http://creativecommons.org/licenses/by/4.0/>.

References

- [1] Tokura Y (ed) (2000) Colossal-magnetoresistance oxide. Gordon & Breach Science Publishers, Amsterdam
- [2] Dagotto E (2003) Nanoscale phase separation and colossal magnetoresistance: the physics of manganites and related compounds. Springer series in solid-state sciences, vol 136. Springer, Berlin
- [3] Tokura Y (2006) Critical features of colossal magnetoresistive manganites. Rep Prog Phys 69:797–851
- [4] Catalan G, Scott JF (2009) Physics and applications of bismuth ferrite. Adv Mater 21:2463–2485
- [5] Mahendiran R, Maignan A, Hebert S, Martin C, Hervieu M, Raveau B, Mitchell JF, Schiffer P (2002) Ultrasharp magnetization steps in perovskite manganites. Phys Rev Lett 89:286602
- [6] Shahee A, Choudhary RJ, Rawat R, Awasthi AM, Lalla NP (2014) Effect of oxygen off-stoichiometry on coupled structural and magnetic phase-transitions in $\text{La}_{0.15}\text{Sr}_{0.85}\text{MnO}_{3-\delta}$ ($\delta = 0.02, 0.14$). Solid State Commun 177:84–88
- [7] Zhou Y, Zhu X, Li S (2015) Effect of particle size on magnetic and electric transport properties of $\text{La}_{0.67}\text{Sr}_{0.33}\text{MnO}_3$ coatings. Phys Chem Chem Phys 17:31161–31169
- [8] Coey JMD, Viret M, von Molnár S (1999) Mixed-valence manganites. Adv Phys 48:167–293
- [9] Millis AJ (1996) Cooperative Jahn–Teller effect and electron–phonon coupling in $\text{La}_{1-x}\text{A}_x\text{MnO}_3$. Phys Rev B 53:8434–8441
- [10] Dagotto E, Hotta T, Moreo A (2001) Colossal magnetoresistant materials: the key role of phase separation. Phys Rep 344:1–153
- [11] Zener C (1951) Interaction between the d-shells in the transition metals. II. Ferromagnetic compounds of manganese with perovskite structure. J Phys Rev 82:403–405
- [12] Raveau B, Hervieu M, Maignan A, Martin C (2001) The route to CMR manganites: what about charge ordering and phase separation? J Mater Chem 11:29–36
- [13] Wang LM, Lai J-H, Wu J, Kuo Y-K, Chang CL (2007) Effects of Ru substitution for Mn on $\text{La}_{0.7}\text{Sr}_{0.3}\text{MnO}_3$ perovskites. J Appl Phys 102:023915
- [14] Thaljaoui R, Boujelben W, Pękała M, Pękała K, Cheikhrouhou Koubaa W, Cheikhrouhou A (2013) Magnetocaloric study of monovalent-doped manganites $\text{Pr}_{0.6}\text{Sr}_{0.4-x}\text{Na}_x\text{MnO}_3$ ($x = 0-0.2$). J Mater Sci 48:3894–3903. <https://doi.org/10.1007/s10853-013-7191-2>
- [15] Thaljaoui R, Boujelben W, Pękała M, Pękała K, Fagnard J-F, Vanderbemden P, Donten M, Cheikhrouhou A (2014) Magnetocaloric effect of monovalent K doped manganites $\text{Pr}_{0.6}\text{Sr}_{0.4-x}\text{K}_x\text{MnO}_3$ ($x = 0$ to 0.2). J Magn Magn Mater 352:6–12

- [16] Thaljaoui R, Boujelben W, Pękała M, Pękała K, Cheikhrouhou A (2013) Structural and electrical properties of monovalent doped manganites $\text{Pr}_{0.6}\text{Sr}_{0.4-x}\text{K}_x\text{MnO}_3$ ($x = 0, 0.05$ and 0.1). *J Supercond Nov Magn* 26:1625–1630
- [17] Thaljaoui R, Boujelben W, Pękała M, Pękała K, Mucha J, Cheikhrouhou A (2013) Structural, magnetic and transport study of monovalent Na-doped manganite $\text{Pr}_{0.55}\text{Na}_{0.05}\text{Sr}_{0.4}\text{MnO}_3$. *J Alloys Compd* 558:236–243
- [18] Thaljaoui R, Boujelben W, Pękała M, Pękała K, Antonowicz J, Fagnard J-F, Vanderbemden P, Dąbrowska S, Mucha J (2014) Structural, magnetic and magneto-transport properties of monovalent doped manganite $\text{Pr}_{0.55}\text{K}_{0.05}\text{Sr}_{0.4}\text{MnO}_3$. *J Alloys Compd* 611:427–432
- [19] Panwar N, Rao A, Singh RS, Syu WK, Kaurav N, Kuo Y-K, Agarwal SK (2008) Magnetotransport, thermoelectric power, thermal conductivity and specific heat of $\text{Pr}_{2/3}\text{Sr}_{1/3}\text{MnO}_3$ manganite. *J Appl Phys* 104:083906
- [20] Tachibana M, Takayama-Muromachi E (2008) Thermal conductivity of colossal magnetoresistive manganites $(\text{La}_{11-x}\text{Nd}_x)_{0.7}\text{Pb}_{0.3}\text{MnO}_3$. *Appl Phys Lett* 92:242507
- [21] Szewczyk D, Thaljaoui R, Mucha J, Stachowiak P, Vanderbemden P (2018) Specific heat and magnetocaloric effect in $\text{Pr}_{0.6}\text{Sr}_{0.4-x}\text{Ag}_x\text{MnO}_3$ manganites. *Intermetallics* 102:88–93
- [22] Jeżowski A, Mucha J, Pompe G (1987) Thermal conductivity of the amorphous alloy $\text{Fe}_{40}\text{Ni}_{40}\text{P}_{14}\text{B}_6$ between 80 and 300 K. *J Phys D Appl Phys* 20:1500–1506
- [23] Daivajna MD, Kumar N, Awana VPS, Gahtori B, Benedict Christopher J, Manjunath SO, Syu KZ, Kuo YK, Rao A (2014) Electrical, magnetic and thermal properties of $\text{Pr}_{0.6-x}\text{Bi}_x\text{Sr}_{0.4}\text{MnO}_3$ manganites. *J Alloys Compd* 588:406–412
- [24] Thaljaoui R, Pękała M, Fagnard J-F, Vanderbemden Ph (2017) Effect of Ag substitution on structural, magnetic and magnetocaloric properties of $\text{Pr}_{0.6}\text{Sr}_{0.4-x}\text{Ag}_x\text{MnO}_3$ manganites. *J Rare Earths* 35:875–882
- [25] Thaljaoui R, Boujelben W, Pękała M, Pocięcha D, Szydłowska J, Cheikhrouhou A (2012) Room temperature magnetocaloric and magneto-transport properties of monovalent doped $\text{Pr}_{0.6}\text{Sr}_{0.35}\text{Na}_{0.05}\text{MnO}_3$ manganite. *J Alloys Compd* 530:138–143
- [26] Venkataiah G, Venugopal Reddy P (2005) Structural, magnetic and magnetotransport behavior of some Nd-based perovskite manganites. *Solid State Commun* 136:114–119
- [27] Gopal Rao TR, Ravi S, Pamu D (2016) Electrical transport and magnetic properties of epitaxial thin films on (001)-oriented LaAlO_3 substrate. *J Magn Magn Mater* 409:148–156
- [28] Xie Q, Lv B, Wang P, Song P, Wu X (2009) Evolution of A-site disorder-dependent structural and magnetic transport properties in $\text{La}_{2/3-x}\text{Eu}_x\text{Ca}_{1/3-y}\text{Sr}_y\text{MnO}_3$. *Mater Chem Phys* 114:636–643
- [29] Solanki PS, Doshi RR, Khachar UD, Vagadia MV, Ravalia AB, Kuberkar DG, Shah NA (2010) Structural, microstructural, transport and magnetotransport properties of nanostructured $\text{La}_{0.7}\text{Sr}_{0.3}\text{MnO}_3$ manganites synthesized by coprecipitation. *J Mater Res* 25:1799–1802
- [30] Li J, Huang Q, Li ZW, You LP, Xu SY, Ong CK (2001) Microstructure modification and magnetoresistance enhancement by Ag doping in $\text{La}_{2/3}\text{Sr}_{1/3}\text{MnO}_3$ thin films prepared by dual-beam pulsed laser ablation. *J Phys Condens Matter* 13:3419–3431
- [31] Berman R (1976) Thermal conduction in solids. Oxford University Press, New York
- [32] Gamzatov AG, Batdalov AB, Aliev AM, Khurshilova Z, Ellouze M, Ben Jemma F (2017) Specific heat, thermal diffusion, thermal conductivity and magnetocaloric effect in $\text{Pr}_{0.6}\text{Sr}_{0.4}\text{Mn}_{1-x}\text{Fe}_x\text{O}_3$. *J Magn Magn Mater* 443:352–357
- [33] Battabyal M, Dey TK (2004) Thermal conductivity of silver doped lanthanum manganites between 10 and 300 K. *J Phys Chem Solids* 65:1895–1900
- [34] Wiedemann G, Franz R (1853) Ueber die Wärme-Leitungsfähigkeit der Metalle. *Annalen der Physik und Chemie* 89:497–531
- [35] Callaway J (1959) Model for lattice thermal conductivity at low temperatures. *Phys Rev* 113:1046–1051
- [36] Oleaga A, Salazar A, Prabhakaran D, Boothroyd AT (2005) Critical behaviour of RMnO_3 ($R = \text{La}, \text{Pr}, \text{Nd}$) by thermal diffusivity and specific heat measurements. *J Phys Condens Matter* 17:6729–6736

Publisher's Note Springer Nature remains neutral with regard to jurisdictional claims in published maps and institutional affiliations.